High-Temperature Ternary Oxide Phases in Tantalum/Niobium–Alumina Composite Materials

Michael K. Eusterholz,* Torben Boll,* Julian Gebauer, Anja Weidner, Alexander Kauffmann, Peter Franke, Hans Jürgen Seifert, Horst Biermann, Christos G. Aneziris, and Martin Heilmaier

Coarse-grained composites of refractory ceramics and refractory metals are a novel approach for materials at application temperatures up to 1500 °C. Al_2O_3 and the refractory metals Nb and Ta are suitable candidates for enhanced thermal shock capability, as they show similar thermal expansion. During fabrication, a key aspect to consider is the possible formation of additional phases upon interaction of the constituent phases as well as through reaction with the environment. X-Ray diffraction (XRD) and investigations of the microstructure with scanning electron microscopy methods unveil Al_2O_3–Nb composite to form NbO, whereas for Al_2O_3–Ta the ternary compound aluminum tantalate ($AlTaO_4$) is found. Thermodynamic calculations show that the changing oxygen solubility in Nb accounts for the formation of NbO, and explain the absence of a corresponding niobate ($AlNbO_4$) phase. $AlTaO_4$ is identified as the disordered tetragonal high-temperature modification.

1. Introduction

Refractory metal (molybdenum, niobium, and tantalum) matrix composite materials in combination with refractory ceramics (alumina, zirconia, and mullite) are of particular interest for high-temperature applications, e.g., in refractory linings in the casting industry.[1] However, besides the high-temperature applicability, other aspects need consideration as well for the choice of material combination, such as: 1) the reaction between the metal and ceramic particles, 2) the chemical interaction with the environment, and 3) the thermal mismatch between the ceramic and the metallic phases.[2] The majority of the past publications dealt with so-called fine-grained refractory composites.[3–7] However, their disadvantages are high shrinkage on sintering, thus resulting in limited thermal shock ability. The refractory metals Nb and Ta are promising candidates for application with Al_2O_3 due to their similar thermal expansion behavior. Wang et al.[8] and White et al.[9] showed for temperatures between 1000 and 2000 K a similarly linear increase of the linear thermal expansion coefficient for the three elements, with 8.8 to $11.2 \times 10^{-6} \, K^{-1}$ for α-Al_2O_3,[8] 8.3 to $10.4 \times 10^{-6} \, K^{-1}$ for Nb, and 7.1 to $8.4 \times 10^{-6} \, K^{-1}$ for Ta.[9] Recently, Zienert et al.[10] demonstrated the fabrication of coarse-grained refractory composites based on alumina with niobium or tantalum, while Weidner et al.[11] reported first mechanical properties at high temperatures (1300–1500 °C) under compressive load. In these coarse-grained refractory composites, alumina with different particle classifications from 0–20 μm up to 2–5 mm (with different volume

M. K. Eusterholz, T. Boll, A. Kauffmann, M. Heilmaier
Institute for Applied Materials – Materials Science and Engineering (IAM-WK)
Karlsruhe Institute of Technology (KIT)
Engelbert-Arnold-Str. 4, 76131 Karlsruhe, Germany
E-mail: michael.eusterholz@kit.edu; torben.boll@kit.edu

M. K. Eusterholz, T. Boll
Institute of Nanotechnology (INT)
Karlsruhe Institute of Technology (KIT)
Hermann-von-Helmholtz-Platz 1, 76344 Eggenstein-Leopoldshafen, Germany

T. Boll
Karlsruhe Nano Micro Facility (KNMFi)
Karlsruhe Institute of Technology (KIT)
Hermann-von-Helmholtz-Platz 1, 76344 Eggenstein-Leopoldshafen, Germany

J. Gebauer, P. Franke, H. J. Seifert
Institute for Applied Materials – Applied Materials Physics (IAM-AWP)
Karlsruhe Institute of Technology (KIT)
Hermann-von-Helmholtz-Platz 1, 76344 Eggenstein-Leopoldshafen, Germany

A. Weidner, H. Biermann
Institute of Materials Engineering
TU Bergakademie Freiberg
Gustav-Zeuner-Str. 5, 09599 Freiberg, Germany

C. G. Aneziris
Institute of Ceramics, Refractories and Composite Materials
TU Bergakademie Freiberg
Agricolastr. 17, 09599 Freiberg, Germany

2200161 (1 of 7)

fractions) was combined with fine metal powders of Ta or Nb ($d \leq 75\,\mu m$). Moreover, Zienert et al.[12] successfully fabricated niobium-alumina aggregate fractions with particle sizes up to 3 mm by crushing pre-synthesized fine-grained composites. A shrinkage of 1.6% was determined for such coarse-grained composites after sintering.

Weidner et al.[11] showed that the coarse-grained Ta–Al_2O_3 and Nb–Al_2O_3 exhibited good mechanical properties depending on the volume fraction of refractory metals and temperature. Thus, compressive strengths of about 70 and 53 MPa were achieved at 1300 °C for 11 vol% Ta and Nb, respectively. 21 vol% metal yielded compressive strength values of 27 and 32 MPa, respectively. None of the tested specimens failed in a brittle manner, in all cases, certain plasticity was observed. However, one or two of the above-addressed issues seem to appear for this class of refractory metal (Nb, Ta) composites: 1) the reaction between the metal and ceramic particles and/ or 2) the chemical interaction with the environment, resulting in the apparent formation of new phases (see Figure 3 and 4 for Ta-composites and Nb-composites, respectively, in Ref. [11]). Earlier literature described the possible formation of such phases in the systems Ta–Al_2O_3[13] and Nb–Al_2O_3.[14] The consolidation of our samples takes place under a protective Ar atmosphere with residual oxygen (in the range of a few ppm) and, additionally, under the presence of different contaminants in the raw materials. One of the conclusions drawn in Ref. [11] based on scanning electron microscope (SEM) investigations was the possible formation of tantalates and niobates during the sintering process in the fabrication route of these materials, but the exact identity of the phases remained unknown. At the time of writing, neither experimental evidence for the existence of these new phases nor thermodynamic calculations were available and will be presented in this article. In addition, it is of interest at which stage during preparation these phases form: During sintering or subsequent mechanical loading at high temperature?

The aims of the present study are thus twofold: 1) experimental analysis of the formed new phases in both systems Ta–Al_2O_3 and Nb–Al_2O_3 and 2) thermodynamic calculations of the formation of these new phases. We conducted microstructural investigations based on XRD and SEM using electron backscattered diffraction (EBSD) in combination with backscattered electron (BSE) contrast for the systems Nb–Al_2O_3 and Ta–Al_2O_3. Thermodynamic calculations of isothermal sections of the ternary phase diagrams Al–Nb–O and Al–Ta–O underpin our investigations.

2. Experimental Section

The refractory ceramic–refractory metal composites investigated in this work were prepared by Zienert et al.[10] from coarse-grained (i.e., coarse particle size) alumina and fine-grained niobium or tantalum, respectively. They were already part of investigations by Weidner et al.[11] The raw materials used are listed in **Table 1**.

Alumina particles from four different classifications were used: 0–0.5 mm (21 vol%), 0.5–1 mm (10 vol%), 1–3 mm (13 vol%), and 2–5 mm (24 vol%). The refractory metals were added as two fine powder fractions, 0–20 μm (10 vol%) and 0–45 μm (11 vol%), yielding a total metal content in the castable

Table 1. Raw materials used for the refractory ceramic-refractory metal composites.

Material	Supplier
Tabular alumina T60/64	Almatis GmbH, Frankfurt, Germany
Reactive alumina CL370	Almatis GmbH
Alumina Martoxid MR-70	Martinswerk GmbH, Bergheim, Germany
Alphabond 300 alumina binder	Almatis GmbH
ADS-1, ADW-1 dispersing alumina	Almatis GmbH
Nb powder (99.95 % purity)	EWG E. Wagener GmbH, Heimsheim, Germany
Ta powder (99.95 % purity)	Haines & Maassen Metallhandelsgesellschaft mbH, Bonn, Germany

of 21 vol%. 8 vol% CL370 and 3 vol% alphabond were used as additives. The powders with a volume of ≈350 cm^3 were mixed in a concrete mixer (ToniMAX, Toni Baustoffprüfsysteme GmbH, Berlin, Germany) using 5 wt% water and 1 wt% of dispersing alumina as additives. The resulting blends were cast into prismatic (150 × 25 × 25 mm^3) sample molds and left to rest for 1–3 days. The samples were removed, dried in air at 120 °C for 24 h, and sintered pressurelessly under an argon atmosphere at 1600 °C for 4 h. The following investigations focus on composite materials containing 21 vol% of Nb or Ta. The investigated samples are hereinafter called 21F0C-Nb and 21F0C-Ta, according to the nomenclature given in Refs. [10,11] For this purpose, the samples were cut parallel to the cylinder axis and embedded one half in EpoMet resin (Buehler, Esslingen am Neckar, Germany), ground to SiC grit P4000, and subsequently polished with 3 and 1 μm diamond suspension. The final polishing was performed with colloidal SiO_2 suspension.

Crystal structure analyses were performed with XRD using a Bruker D2 phaser in Bragg–Brentano geometry with Cu K_α radiation at a step size of 0.01°. For electron microscopy imaging and EBSD the dual-beam scanning electron and focused ion beam microscope Zeiss Auriga 60 (Carl Zeiss AG, Oberkochen, Germany) was used equipped with a BSE imaging detector and an EDAX DigiView EBSD camera. The BSE images at three different contrast levels were used for phase segmentation based on gray-level binarization, employing a self-programmed MATLAB script, and compared to EBSD at 20 kV. Oxygen contents of the metals were determined with atom probe tomography (APT) measurements in a LEAP 4000X HR by Came
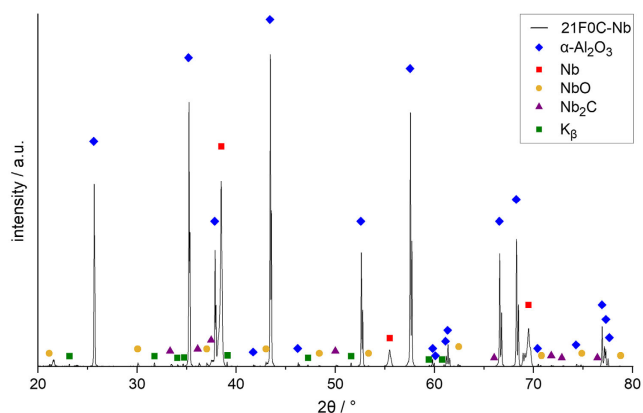
Isothermal sections of the Al–Ta–O and Al–Nb–O ternary system at 1600 °C were obtained by CALPHAD modeling as described in Ref. [15].

3. Results

3.1. XRD

XRD phase analysis was performed for both, the 21F0C-Nb and 21F0C-Ta samples.

Figure 1 shows the XRD line profile of 21F0C-Nb and confirms the presence of α-Al_2O_3 (blue diamond symbols, corundum prototype, and space group 167), Nb (red squares,

**ADVANCED
SCIENCE NEWS**
www.advancedsciencenews.com

**ADVANCED
ENGINEERING
MATERIALS**
www.aem-journal.com

Figure 1. XRD pattern of 21F0C-Nb. α-Al_2O_3 (space group 167), Nb (space group 229), NbO (space group 221), and Nb_2C (space group 6, 33, or 149) were found. Minor peaks remain unassigned and may arise from castable additives.

W prototype, and space group 229), and NbO (yellow circles, NbO prototype, and space group 221), with the characteristic peaks of the latter at $2\theta = 30.0°$, $48.3°$, and $62.4°$. In addition, the crystallographic data matches different modifications of Nb_2C (violet triangles) of the monoclinic (space group 6) and the orthorhombic (space group 33) variants, as well as of the hexagonal superstructure originally reported by Terao[16] (ϵ-Fe_2N prototype, space group 149). No unequivocal assignment to any of these prototypes is possible based on the assigned peaks at $2\theta = 33.5°$, $36.8°$, and $50.1°$. While the peaks labeled by green squares result from K_β diffraction, a few unidentified peaks remain, which may result from contaminations in the castable additives, notably the alumina binder, which contains traces of Na_2O, SiO_2, and CaO. No evidence of niobates (e.g., $AlNbO_4$) was found from XRD measurements.

For the 21F0C-Ta composite, XRD (**Figure 2**) confirms the presence of α-Al_2O_3, Ta, and, as Weidner et al.[10] suggested, the ternary oxide $AlTaO_4$ (aluminum tantalate, TiO_2 prototype, space group 136) with characteristic peaks at $2\theta = 27.4°$, $35.8°$,
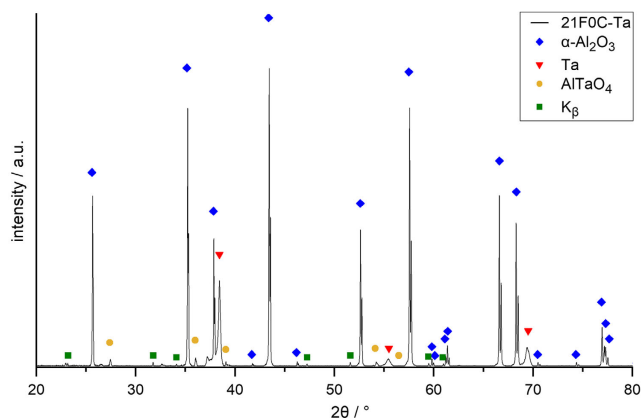

Figure 2. X-Ray diffraction (XRD) pattern of 21F0C-Ta. Besides α-Al_2O_3 (space group 167) and Ta (space group 229), $AlTaO_4$ (space group 136) was found. For some minor peaks, $NaTaO_3$ (space group 62) ($2\theta = 32.6°$) and TaH ($2\theta = 37.2°$) are possible candidates.

and $39.1°$. K_β signals are again marked in green, while a few peaks remain unassigned. A possible candidate for the unassigned peaks at $2\theta = 23.0°$ and $32.6°$ is sodium tantalate ($NaTaO_3$), with castable additives and Na contamination in the alumina as a sodium source.[17]

3.2. Microstructural Investigations

To study the presence of additional phases such as NbO or niobates and tantalates, as suggested by Weidner et al.,[11] SEM investigations were performed using BSE contrast and EBSD measurements.

Figure 3 depicts a phase segmentation micrograph of 21F0C-Nb. The three BSE images used can be found in the Figure S1, Supporting Information. A mixture of coarse-grained alumina (blue) particles and Nb (red) particles with metal grain sizes ranging from a few microns to up to 75 μm is visible. In addition, fine-grained alumina particles are present in between Nb particles. In yellow, an intermediate BSE contrast is assigned to an additional phase, which was suggested in Ref. [11] to be either NbO or Al niobate ($AlNbO_4$) based on SEM-EDS measurements. This will be further discussed in the context of **Figure 4**. Black areas are related to porosity remaining in the material after the sintering process. The lack of different contrast levels suggests that no additional phase is present within the resolution of the technique. Phase segmentations performed in these regions yield an average Nb volume fraction of about (27 ± 1) vol.-% and an alumina fraction of (44 ± 4) vol%. Porosity was determined to be (27 ± 4) vol%. The suspected NbO makes up roughly (0.2 ± 0.05) vol%, with a NbO/Nb ratio of 0.007 ± 0.001, and is located within or at Nb particles. Areal phase fractions are regarded to be equivalent to volume fractions due to the isotropy of the microstructure. However, the local heterogeneity of the material has to be taken into account, and, therefore, a single image resolving the finely distributed tertiary phase cannot be representative. Weidner et al.[11] mentioned an average porosity of about 17 vol% measured with the Archimedes principle for the complete sample, which gives a more representative value for the typical material than the 27 vol% obtained from local 2D SEM investigation but considers only open porosity. Due to higher shrinkage, porosity is more significant in regions with large amounts of fine-grained material. When only considering
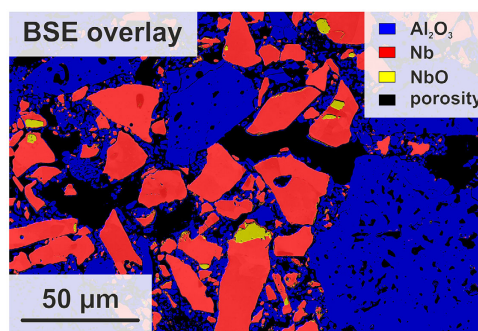
Figure 3. Phase segmentation from backscattered electron (BSE) based on gray-level binarization. The phases α-Al_2O_3, Nb, NbO, as well as porosity, are indicated.
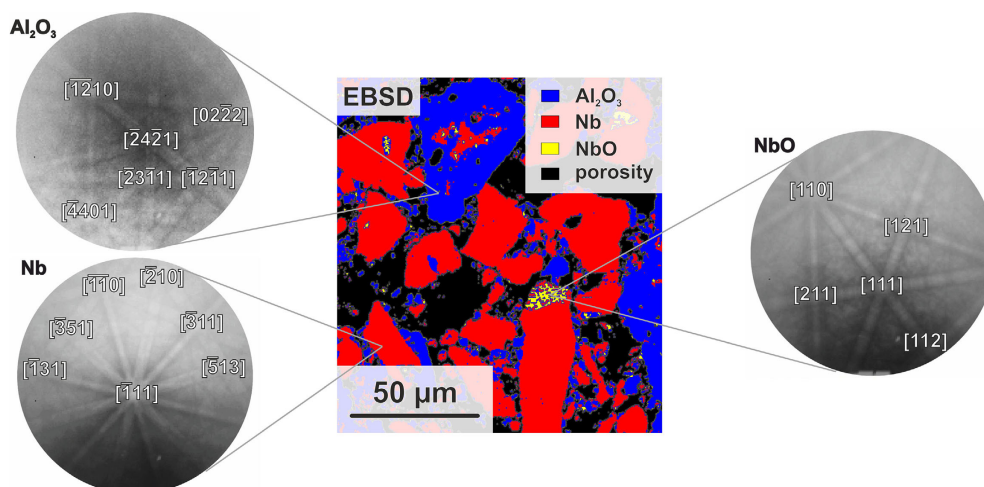
Figure 4. Electron backscattered diffraction (EBSD) map of a section displayed in Figure 3 with electron backscatter diffraction patterns (EBSPs) for the phases α-Al$_2$O$_3$, Nb, and NbO.

coarse-grained alumina regions, the porosity measured with phase segmentation from SEM is 15 vol% and below.

Additional EBSD measurements confirmed the presence of the suspected NbO or AlNbO$_4$ phases. The EBSD phase map and the electron backscatter diffraction patterns (EBSP) shown in Figure 4 confirm that the different phases indicated in Figure 3 correspond to α-Al$_2$O$_3$, Nb, and NbO. Thus, no evidence of AlNbO$_4$ was found from EBSD measurements. When compared to Figure 3, some falsely assigned pixels in the EBSD map occur. This is due to unfavorable grain orientations and insufficient surface finish in certain regions, which stems from the largely varying strength and hardness of the phases involved.

Figure 5 depicts a representative region of the microstructure of 21F0C-Ta with Ta particles (red) mixed with a smaller fraction of alumina and neighbored by two major alumina particles (blue). The BSE images used for phase segmentation can be found in Figure S2, Supporting Information. Regions of a third, intermediate contrast in the vicinity of Al$_2$O$_3$ and Ta are colored yellow and are assigned to AlTaO$_4$. As an average of three-phase segmentation, we find a Ta volume fraction of about (17 ± 2) % and an alumina fraction of (56 ± 5) vol%. The porosity amounts to (22 ± 3) vol%, while the AlTaO$_4$ phase fraction is
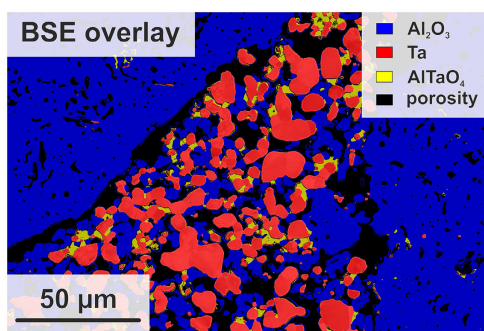
(0.2 ± 0.06) vol%. The ratio of ternary oxide to the refractory metal Ta amounts to 0.012 ± 0.002, which is considerably more than the NbO/Nb ratio in 21F0C-Nb. Similar to the Nb-containing composite, the heterogeneity of the material again complicates the determination of phase fractions. While Ta roughly corresponds to the initial amount of 21 vol%, the alumina fraction is lower than the amount in the castable. In coarse-grained alumina regions, the Al$_2$O$_3$ content exceeds values of 75 vol%. The observed porosity is roughly in the range of 17 vol%., as reported by Weidner et al.[11]

The region depicted in Figure 5 was examined with EBSD to confirm the phase assignments. **Figure 6** features a phase map of the region with EBSPs of all the phases present, i.e., Al$_2$O$_3$ (blue), Ta (red), and AlTaO$_4$ (yellow), which confirms the findings from X-Ray diffraction. Predominantly within the oxides, some Al$_2$O$_3$ regions were falsely assigned to AlTaO$_4$ due to poor Kikuchi pattern quality. These also do not appear as respective contrast for the phase segmentation map in Figure 5.

3.3. Thermodynamic Considerations

A discussion of the phases present in the microstructure of the refractory composites requires the phase diagrams of the systems Al–Nb–O and Al–Ta–O at the sintering temperature (1600 °C). These diagrams are not available in the literature and must be calculated using appropriate thermodynamic databases. Using the well-known CALPHAD method,[15] Gebauer et al.[18] assess thermodynamic datasets for both ternary systems. The databases consist of Gibbs energy functions that are temperature, pressure, and composition dependent. Thermodynamic equilibria are calculated by evaluating these functions for specified condition sets. Isothermal sections are then obtained by evaluating these equilibria at a given temperature for two independent composition variables. This dataset considers phase descriptions for intermetallic phases, binary and ternary oxides, and an emphasis on the quasi-binary section Al$_2$O$_3$–Nb$_2$O$_5$. **Figure 7** shows the calculated isothermal section at 1600 °C and standard pressure for the Al–Nb–O system. At this
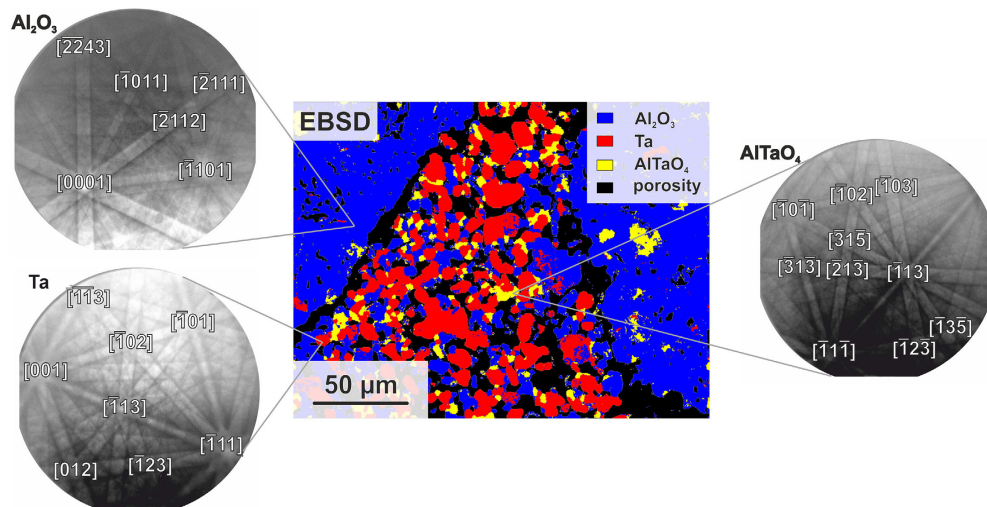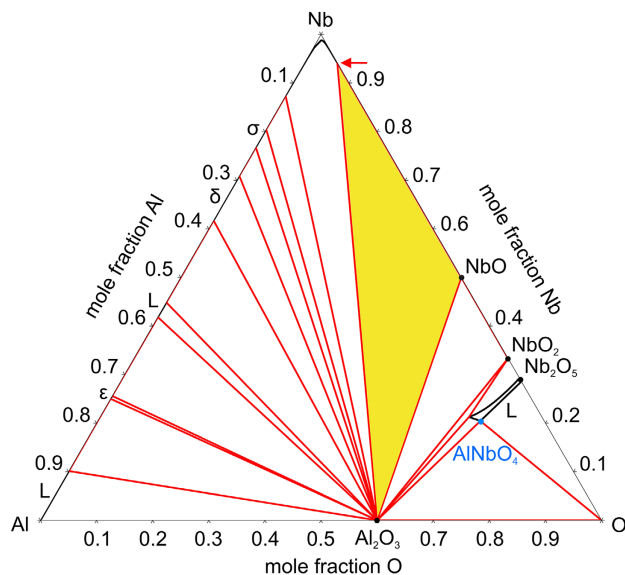

Figure 5. Phase segmentation from BSE. The phases α-Al$_2$O$_3$, Ta, and AlTaO$_4$, as well as porosity, are indicated by red, blue, yellow color, and black, respectively.
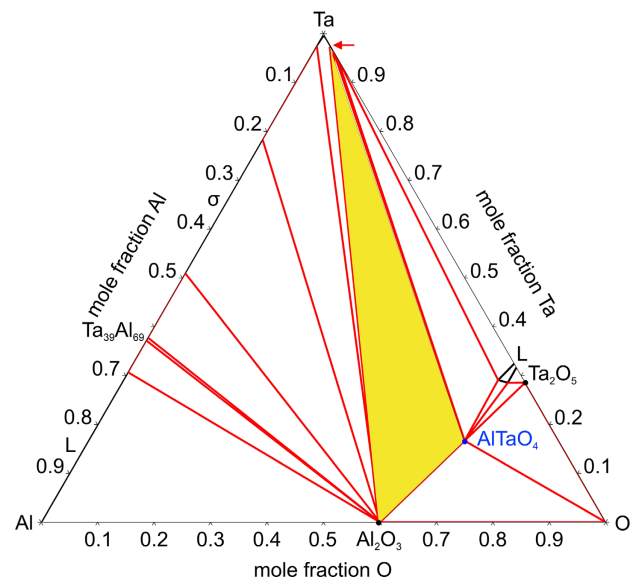
Figure 6. EBSD map of the region shown in Figure 5 with EBSPs for the phases α-Al₂O₃, Ta, and AlTaO₄.

Figure 7. Calculated isothermal section of the ternary Al–Nb–O system at 1600 °C and 10^5 Pa. L denotes liquid phase regions, whereas ε, δ, and σ are Al–Nb intermetallic phases. The three-phase region Nb–Al₂O₃–NbO is marked yellow.

Figure 8. Calculated isothermal section of the ternary Al–Ta–O system at 1600 °C and 10^5 Pa. L denotes liquid phase regions, whereas σ is an Al–Ta intermetallic phase. The three-phase region Ta–Al₂O₃–NbO is marked yellow.

temperature, the maximum oxygen solubility in Nb, indicated by a red arrow, is about 6 at% but will decrease with decreasing temperature.[19] APT measurements (see Figure S3, Supporting Information) in the Nb particles indeed yield a lower value of (3.0 ± 0.2) at% which corresponds to the solubility at about 1200 °C.[19]

For the Al–Ta–O ternary system, the calculated isothermal section at 1600 °C and standard pressure show an oxygen solubility of about 5 at% in Ta, indicated by the red arrow in **Figure 8**. As for Nb, this value decreases with decreasing temperature.[20] With APT measurements (see Figure S4, Supporting Information), we found an oxygen content of (3.2 ± 0.075) at% in Ta particles.

4. Discussion

The above-presented results of XRD and SEM have shown that reactions between the refractory metal and ceramic particles and/or possibly the chemical interaction with the environment lead to the formation of AlTaO₄ in the system Ta–Al₂O₃ and NbO in the system Nb–Al₂O₃. Figure 1 and 2, moreover, indicate that these newly formed phases are not localized but are found throughout the material. Comparison of Figure 3 and 5 shows that NbO is present within or at Nb particles. In contrast, the phase identified as AlTaO₄ is adjacent to both Al₂O₃ and Ta, suggesting a reaction involving alumina. Further phases, such as Nb₂C, found in small amounts with XRD, could not be recognized with SEM methods.

**ADVANCED
SCIENCE NEWS**

www.advancedsciencenews.com

**ADVANCED
ENGINEERING
MATERIALS**

www.aem-journal.com

The findings that these additional phases form during sintering are supported by thermodynamical considerations using the CALPHAD method. Whereas some NbO was already found in the original Nb powder,[12] its presence in the composites can be attributed to additional oxygen uptake of the samples during the sintering process, as is shown in Figure 7. The oxygen concentration of (3.0 ± 0.2) at% found in Nb with APT is considerably lower than the solubility limit of 6 at% at 1600 °C and corresponds to the limit at about 1200 °C. Thus, due to this decrease during cooling in the sintering furnace, an initially two-phase Nb–Al$_2$O$_3$ composite with 6 at% O in the metallic particles will form NbO, as the phase region boundary Nb–Al$_2$O$_3$ moves to the left upon cooling and the three-phase region marked in yellow extends to lower oxygen fractions. Several possible sources, like the sintering atmosphere, but also castable additives, e.g., water, may account for the increased oxygen level. Figure 7, moreover, shows why no ternary Al–Nb–O compound (aluminum niobate, AlNbO$_4$, space group 12, indicated in blue) is formed, as it is not stable in the presence of metallic Nb. According to Figure 7, AlNbO$_4$ is obtained through a reaction of Al$_2$O$_3$ and Nb$_2$O$_5$. Thus, the absence of the niobate precludes the occurrence of the latter during sintering. The experimentally determined occurrence of NbO, thus, matches the calculated three-phase equilibrium Nb–Al$_2$O$_3$–NbO from the database presented by Gebauer et al.[18]

Likewise, the experimental findings match calculations of the ternary system Al–Ta–O. Thus, as for Al–Nb–O, during cooling, the decrease of the oxygen solubility in the metallic regions, i.e., an extension of the yellow three-phase region to smaller oxygen fractions, will induce the formation of an additional oxide phase. However, unlike for Al–Nb–O, where NbO coexists with Al$_2$O$_3$ and Nb, here, it is the mixed oxide AlTaO$_4$ that shares a three-phase field with Al$_2$O$_3$ and Ta. Furthermore, this compound can be obtained through a reaction of Al$_2$O$_3$ with Ta$_2$O$_5$,[13] as shown in Figure 8. This oxide may have formed through partial oxidation of the metal powder during the heat treatment but was not found in our investigations.

Notably, for the presented specimen, XRD and EBSD confirm that the structure of AlTaO$_4$ is tetragonal. Ternary oxometallates of the formula AlMO$_4$ (with M = Nb, Ta, among others) crystallize in a monoclinic crystal structure of the AlNbO$_4$ prototype (space group 12).[21–23] However, Jasper-Tönnies and Müller-Buschbaum,[13] as well as Sarazin in an earlier publication,[24] reported the formation of an additional metastable tetragonal rutile-type AlTaO$_4$ from Al$_2$O$_3$ (corundum) and Ta$_2$O$_5$ in the temperature range of 1300–1400 °C, and at 1800 °C. Roth et al.[25] and Wichmann et al.[26] correlated the preferred formation of this modification to a decrease in the Coulomb contribution of the lattice energy, i.e., to entropy stabilization through disorder concerning the lattice positions of the metals. Thus, similar to the VO$_2$ system,[27] besides the low-temperature monoclinic form, a disordered high-temperature modification of AlTaO$_4$ exists. Our results confirm the formation of this ternary metastable AlTaO$_4$ (space group 136) modification in Al$_2$O$_3$- and Ta-containing samples subjected to a sintering temperature of 1600 °C for 4 h. Rutile-type tantalate compounds may furthermore be a path to enhance oxidation resistance of the underlying metal. CrNbO$_4$ and CrTaO$_4$ have been found to form dense, protective layers in refractory high-entropy alloy oxides scales.[28–31]

Investigation of AlTaO$_4$ in this regard may be promising, whereas no rutile-type compound is known in the Al–Nb–O system.

5. Conclusions

Refractory composites of alumina and a refractory metal (Nb or Ta) form oxide phases during sintering at 1600 °C. XRD, BSE, and EBSD results confirm the phases predicted by CALPHAD calculations to be NbO or AlTaO$_4$ for the Nb- or Ta-containing composite, respectively. The composites were produced from a mixture containing 21 vol% metal, alumina, and binder. Traces of Nb$_2$C were observed for the Nb-composite with XRD. NbO directly forms due to excess oxygen, while no Ta oxides were found. This can be explained by a possible reaction path for AlTaO$_4$, which consumes Ta$_2$O$_5$. AlTaO$_4$ is present in the tetragonal high-temperature modification as grains at the alumina–metal interface. As expected from the calculations, a corresponding aluminum niobate (AlNbO$_4$) was not found experimentally. This compound forms through a reaction of Al$_2$O$_3$ and Nb$_2$O$_5$, thus, its absence rules out the occurrence of the pentoxide.

Conflict of Interest

The authors declare no conflict of interest.

Data Availability Statement

The data that support the findings of this study are available from the corresponding author upon reasonable request.

[1] C. Sadik, I.-E. El Amrani, A. Albizane, *J. Asian Ceram. Soc.* **2014**, *2*, 83.

[2] C. G. Aneziris, F. Homola, D. Borzov, *Adv. Eng. Mater.* **2004**, *6*, 562.

[3] M. K. Ferber, M. G. Jenkins, V. J. Tennery, in *Ceram. Eng. Sci. Proc. I* annual conference on composites and advanced ceramics, Cocoa Beach, FL (USA), 14–17 January **1990**, pp. 1028–1045.

[4] A. G. Robertson, D. S. Wilkinson, C. H. Caceres, *J. Am. Ceram. Soc.* **1991**, *74*, 915.

[5] C. Scheu, G. Dehm, W. D. Kaplan, F. Wagner, N. Claussen, *Phys. Status Solidi.* **1998**, *166*, 241.

[6] K. E. Thomson, D. Jiang, J. A. Lemberg, K. J. Koester, R. O. Ritchie, A. K. Mukherjee, *Mater. Sci. Eng. A* **2008**, *493*, 256.

[7] J. S. Moya, M. Díaz, C. F. Gutiérrez-González, L. A. Diaz, R. Torrecillas, J. F. Bartolomé, *J. Eur. Ceram. Soc.* **2008**, *28*, 479.

[8] K. Wang, R. R. Reeber, *Mater. Sci. Eng. R Rep.* **1998**, *23*, 101.

[9] G. K. White, R. B. Roberts, *High Temp. Press.* **1983**, *15*, 321.

[10] T. Zienert, M. Farhani, S. Dudczig, C. G. Aneziris, *Ceram. Int.* **2018**, *44*, 16809.

[11] A. Weidner, Y. Ranglack-Klemm, T. Zienert, C. G. Aneziris, H. Biermann, *Materials* **2019**, *12*, 3927.

[12] T. Zienert, D. Endler, J. Hubálková, G. Günay, A. Weidner, H. Biermann, B. Kraft, S. Wagner, C. G. Aneziris, *Materials* **2021**, *14*, 6453.

[13] H. K. Jasper-Tönnies, B. Müller-Buschbaum, *Zeitschrift Für Anorg. Und Allg. Chem.* **1983**, *116*, 113.

[14] A. M. Sych, A. M. Golub, *Russ. Chem. Rev.* **1977**, *46*, 210.

[15] B. Sundman, H. L. Lukas, S. G. Fries, *Computational Thermodynamics: The Calphad Method*, Cambridge University Press, Cambridge **2007**.

[16] N. Terao, *Jpn. J. Appl. Phys.* **1964**, *3*, 104.

[17] C. B. Carter, M. G. Norton, *Ceramic Materials: Science and Engineering*, Springer Science+Business Media, LLC,, New York, NY **2007**, p. 351.

[18] J. Gebauer, P. Franke, *Adv. Eng. Mater.* **2022**, submitted for the same Special Issue ("Refractory Composites") (Research Unit FOR 3010).

[19] B. Predel, *Nb-O (Niobium-Oxygen): Datasheet From Landolt-Börnstein – Group IV Physical Chemistry*, Vol. *5H: "Li-Mg - Nd-Zr,"*, Springer-Verlag, Berlin Heidelberg **1997**.

[20] S. P. Garg, N. Krishnamurthy, A. Awasthi, M. Venkatraman, *J. Phase Equilibr.* **1996**, *17*, 63.

[21] B. F. Pedersen, *Acta Chem. Scand.* **1962**, *16*, 421.

[22] O. Harneit, H. K. Müller-Buschbaum, *Zeitschrift Für Anorg. Und Allg. Chem.* **1991**, *596*, 107.

[23] M. Ardit, M. Dondi, G. Cruciani, *Am. Mineral.* **2012**, *97*, 910.

[24] G. Sarazin, *C. R. Acad. Sci.* **1959**, *248*, 815.

[25] R. S. Roth, J. L. Waring, *Am. Mineral. J. Earth Planet. Mater.* **1964**, *49*, 242.

[26] R. Wichmann, H. Müller-Buschbaum, *Zeitschrift Für Anorg. Und Allg. Chemie.* **1983**, *503*, 101.

[27] K. D. Rogers, *Powder Diffr.* **1993**, *8*, 240.

[28] B. Gorr, F. Müller, M. Azim, H. J. Christ, T. Müller, H. Chen, A. Kauffmann, M. Heilmaier, *Oxid. Met.* **2017**, *88*, 339.

[29] F. Müller, B. Gorr, H. J. Christ, J. Müller, B. Butz, H. Chen, A. Kauffmann, M. Heilmaier, *Corros. Sci.* **2019**, *159*, 108161.

[30] S. Schellert, B. Gorr, H. J. Christ, C. Pritzel, S. Laube, A. Kauffmann, M. Heilmaier, *Oxid. Met.* **2021**, *96*, 333.

[31] S. Schellert, B. Gorr, S. Laube, A. Kauffmann, M. Heilmaier, H. J. Christ, *Corros. Sci.* **2021**, *192*, 109861.